THE UNIVERSITY OF MICHIGAN

College of Engineering

Department of Mechanical Engineering

Cavitation and Multiphase Flow Laboratory

Report No. UMICH 03371-13-T

MATHEMATICAL MODELLING OF NORMAL IMPACT BETWEEN A FINITE CYLINDRICAL LIQUID JET AND NON-SLIP FLAT RIGID SURFACE

by

Yen C. Huang*

F. G. Hammitt**

Wen-Jei Yang***

(Submitted for Publication to 1st International Symposium on Jet Cutting Technology
British Hydrodynamics Research Association)

Financial Support Provided by:

National Science Foundation
Grant No. GK-730

October 1971

*Former Research Associate and Doctoral Candidate
**Professor-In-Charge, Cavitation and Multiphase Flow Laboratory
***Professor

SUMMARY

The hydrodynamic phenomena for a flat-ended cylindrical water jet of finite length following a normal impact on a rigid plane is studied. The governing partial differential equations of compressible flow, neglecting body force, viscosity and surface tension, are solved numerically by a newly-developed Compressible-Cell-and-Marker (ComCAM) solution method.

Pressure build-up and lateral flow begin simultaneously with the impact. A zone of negative pressure later appears in the upper region of the finite cylindrical jet, but there is no "bursting out" of the back surface, as might be expected. The maximum pressure in the finite cylindrical jet impact is found to be less than the one-dimensional maximum pressure, but the maximum lateral velocity is greater than the impact velocity. As time elapses, the peak pressure on the impact surface shifts from the center radially outward, while the pressure at the center attenuates to the stagnation pressure. The high pressure generated by the impulsive deceleration during the very initial unsteady state portion of the impact is believed to be the most important factor in the destructive action which results.

NOMENCLATURE

Symbol	Description
A	Exponent in Tait's equation of state
B	Constant in Tait's equation of state
C	Shock wave velocity
C_o	Sonic Velocity
D^o	Diameter
H_1, H_2	Dimensions of Computation Domain in z- and r-direction, respectively
K	Constant
L	Length
M	Mach number
p	Pressure
p^o	$p/\rho_o C_o V_o$
R	Radius
R_m	Location of marker m in r- coordinate
r	Radial coordinate
r^o	r/R
t	Time
t^o	Non-dimensional time, Ct/D
U	Marker velocity component in z-direction
u	Velocity component in z-direction
u_n	Velocity component in normal direction
V	Marker velocity component in r- direction
v	Velocity component in r- direction
v_t	Velocity component in tangential direction
V_o	Impact Velocity
x_n	Coordinate in normal direction
x_t	Coordinate in tangential direction
z	Vertical coordinate
z^o	z/L
Z_m	Location of marker m in z-coordinate
α	Stability factor
ρ	Density
Δ	Increment
	Subscripts
c	Characteristic parameter
m	Marker index
n	Normal direction
o	Initial value
t	Tangential direction
	Superscripts
o	Non-dimensional variable

I. INTRODUCTION

When a cylindrical free jet of water is directed against a rigid smooth wall, the jet is deflected into lateral flow parallel to the wall away from the point of impact. Most previous studies of this problem deal with the steady state. Bernoulli's theorem is often used to simplify the analysis for regions away from the stagnation point. Approximately uniform lateral velocity and pressure are predicted. Thickness of lateral flow is all that remains to be determined (Ref. 1). For the region near the stagnation point, the velocity distribution conventionally is assumed, and then pressure is calculated by potential flow theory (Ref. 2).

However, at the first instant of impact, the sudden change of boundary velocity will establish large pressure gradients, which later produce a sudden change in the velocity at every point of the fluid. The velocities and their spatial gradients are negligible compared to the local acceleration in this impulsive motion. Problems involving a sudden change of velocity at a portion of the boundary, similar to the present case, arise in connection with the impact of a liquid jet on the solid surface of a target or a projectile on the free surface of a stationary body of liquid. A severe local pressure of the order of 5000atm. is predicted over a very short duration of 0.20×10^{-6} sec. for an impact velocity of 1000 ft/sec. as an example.

The main objective of the present study was to investigate analytically the environment leading to the destructive action due to a cylindrical jet impingement at high speed. The transient, two-dimensional governing equations plus equation of state for water were formulated. Then, using numerical techniques, the flow patterns, impact pressure and velocity distribution were solved as a function of time following the head-on collision of a cylindrical jet with a rigid plane.

II. ANALYSIS

When a free cylindrical jet of water impinges on a rigid surface, the water is diverted into lateral flow. Equations and boundary conditions describing the situation are well-known, but it is a formidable and probably impossible task to obtain a closed form solution. However, a numerical approach wherein one treats the liquid as a distributed system, subjected to the boundary condition at the interface with solid and gas, is possible.

The compressibility of the liquid must be taken into account in any valid and realistic analysis, since otherwise an unrealistic infinitely large pressure will be produced at the first instant of impact. Unless the impact velocity is extremely small, compressibility effects predominate in the liquid response during the period of unsteadiness. However, it is reasonable to neglect the effect of body force and viscosity as can be easily shown by comparing with impact pressure magnitude. Surface tension which affects the boundary condition can also be neglected. Cylindrical coordinates are natural for the problem. Then the governing equations for a cylindrical liquid jet colliding with a rigid solid surface are as follows.

Continuity and momentum for the liquid gives:

$$\frac{\partial \rho}{\partial t} + \frac{\partial (\rho u)}{\partial z} + \frac{1}{r}\frac{\partial (r\rho v)}{\partial r} = 0 \tag{1}$$

$$\frac{\partial (\rho u)}{\partial t} + \frac{\partial (\rho u^2)}{\partial z} + \frac{1}{r}\frac{\partial (r\rho vu)}{\partial r} = -\frac{\partial p}{\partial z} \tag{2}$$

$$\frac{\partial (\rho v)}{\partial t} + \frac{\partial (\rho uv)}{\partial z} + \frac{1}{r}\frac{\partial (r\rho v^2)}{\partial r} = -\frac{\partial p}{\partial r} \tag{3}$$

and Tait's equation of state for water (Ref. 3) is:

$$\frac{p + B}{p_o + B} = \left(\frac{\rho}{\rho_o}\right)^A \tag{4}$$

u and v are the axial and radial velocity components respectively for the cylindrical coordinates z and r. Time t is another independent variable, and ρ and p are the fluid density and pressure. The values of A and B in Tait's equation of state for water

are chosen as Cole (Ref. 4):

$$A = 7.15 \text{ and } B = 3.047 \text{ kilobars.}$$

The above set of (1) through (4), which are in the Eulerian form, are used to find impact pressure and velocity distribution within the liquid.

The following set of equations for marker particles, which are in Lagrangian form, are required to indicate the movement and location of the liquid boundary.

$$\frac{d(\rho U)}{dt} = -\frac{dp}{dz} \tag{5}$$

$$\frac{d(\rho V)}{dt} = -\frac{dp}{dr} \tag{6}$$

$$Z_m = \int U dt \tag{7}$$

$$R_m = \int V dt \tag{8}$$

Here, U and V are the marker velocity components in the z- and r- direction, while Z_m and R_m denote the coordinates in these directions.

The appropriate initial conditions over the domain of calculation are

$$p = p_o \qquad u = u_o \qquad v = v_o$$

where p_o is the ambient pressure, and u_o and v_o are the initial impact velocities in the z- and r- direction respectively. In the case of a normal impact (i.e., perpendicular), $v_o = 0$ of course and $V_o = u_o$, where V_o is the impact velocity.

The appropriate boundary conditions are:

i) along the axis of symmetry (z), r = 0, and symmetry requires

$$v = 0, \quad \frac{\delta u}{\delta r} = 0, \quad \frac{\delta p}{\delta r} = 0$$

ii) along the impacted rigid surface v = 0, u = 0, $\frac{\delta p}{\delta z} = 0$ for a non-slip wall condition. We have already treated the full-slip boundary condition elsewhere (Ref. 5).

iii) along the free surface, the incompressible continuity condition yields

$$p = p_o, \quad \frac{\delta u_n}{\delta x_n} = \frac{\delta v_t}{\delta x_t} = 0$$

where u_n and v_t are the moving velocity components of the liquid-air interface in the normal x_n and tangential x_t directions of the surface respectively.

iv) along the sides of the finite computational domain, permeable boundary conditions will be imposed, in such a way that the normal space derivative of the variable vanishes at the boundary,

$$\frac{\delta u}{\delta z} = 0, \quad \frac{\delta v}{\delta z} = 0, \quad \frac{\delta p}{\delta z} = 0 \text{ at } z = H_1$$

$$\frac{\delta u}{\delta r} = 0, \quad \frac{\delta v}{\delta r} = 0, \quad \frac{\delta p}{\delta r} = 0 \text{ at } r = H_2$$

where H_1 and H_2 are the dimensions of the computational domain in the z- and r- direction, respectively.

All the above equations are then nondimensionalized and expressed in finite difference forms. A compressible-cell-and-marker numerical solution method was developed (Ref. 6). The numerical computation starts with marker particles located along the interface to keep track of the deformation of the liquid boundary. Then pressure and velocity within the liquid boundary are calculated. The detailed descriptions of the method are given by the first author of the present paper, Huang (Ref. 6).

The numerical results represent approximate solutions to the original differential equations, since derivatives are replaced by finite differences. Terms of the order of the square of the time increment and spatial step size are neglected. The convergence of the finite difference representation, i.e., the degree to which the

approximate solution spproaches the exact solution, must then be examined.

It is known that although the explicit formulation avoids the need of iterative or matrix inversion techniques, the Courant stability criterion (Ref. 7), must be satisfied, i.e., the distance a wave travels in the time increment Δt must be less than the spatial step size Δz or Δr. That is:

$$\Delta t < \frac{\text{min. } (\Delta z, \Delta r)}{C} \tag{9}$$

where C is the shock wave velocity in the liquid phase. With the definition of the stability factor

$$\alpha = \frac{C\Delta t}{\text{min. } (\Delta z, \Delta r)} \tag{10}$$

one can satisfy criterion by selecting a value of α less than unity.

Numerical experiments were carried out to determine the stability factor and required numbers of cells so that convergence of the result was reasonably assured, in regard to magnitudes, timing, and wave shapes. For the actual study, a stability factor $\alpha = 0.1$ and 20 x 40 mesh were used.

III RESULTS AND DISCUSSION

In examining the results, one must consider the following. Constant atmospheric pressure at the water-air free surface is imposed. The impact plane is perfectly rigid, flat and imposes a non-slip boundary condition on the impacting fluid. The water is assumed inviscid, without surface tension, but compressible and elastic. The fracture strength of water is taken to be 270 atm., an experimental result of Briggs (Ref. 8). Of course, ordinarily pure water will rupture at much smaller tensions, but perhaps not for the very short duration of tension involved here. The initial length of the cylindrical droplet is L and its diameter, D. The impact Mach number M is defined as V_o/C_o, where C_o is the sonic velocity in the undisturbed liquid. Two cases with different Mach numbers, namely 0.2 and 0.5, are solved, and then results are plotted on the same figure for better comparison.

Fig. 1 shows how the shape of a droplet with L/D = 1 deforms as a function of time. The top of the droplet retains its original flat shape during the initial period of impact after which it becomes convex. The liquid flows out radially parallel to the surface. It is seen here that the higher the Mach number, the higher the effect of compressibility.

Figs. 2a through 2d depict the isobar distribution in the droplet at various instants, i.e., $t^o = 0.125$, 0.25, 1.0 and 2.5, respectively. The figures illustrate how the pressure waves propagate with time from the impacted surface toward the air-water free surface. Due to constant atmospheric pressure at this free surface, all the isobaric surfaces at small times appear as an inverted cup resting upon the impacted surface (Fig. 2a). As time progresses and the droplet shrinks in height accompanied by radial-expansion (Fig. 2b), each cup-shaped isobaric surface grows in size, both depth and width. The isobaric surfaces for small values of $p^o = p/\rho_o C_o V_o$ still retain the inverted cup shape in the outer region of the droplet, those for medium pressure (in the inner portion) will form egg-shaped surfaces, coaxially arranged, with the smaller end pointing toward the impacted surface, because the pressure on the impact surface is released from the contact edge of solid-liquid interface.

Fig. 2c for $t^o = 1.0$ indicates the possibility of cavitation for Mach 0.2 in that there is a region of negative pressure enclosed by the zero isobaric surface as a result of the rarefaction waves. However, no "bursting out" of the top surface appears. The isobaric surface of $p^o = 0.175$ forms a half-doughnut shape which includes the region of high compressive pressure. Higher pressures are generated by higher impact velocities.

In Fig. 2d ($t^o = 2.5$) the droplet shape has become that of a military helmet. The isobaric surfaces along the axis changes from convex to concave as p^o increases. The

highest p^o values are confined to the half doughnut shape region over the solid surface near $r^o (= r/R) = 1.0$. Greater deformations are observed for higher impact velocities.

Better illustrations of the pressure distribution on the impacted surface and along the axis of symmetry are given in Figs. 3 and 4, respectively. Fig. 3 shows that the pressures build up immediately rather uniformly over the entire impacted surface except near the outer edge, where the boundary condition of atmospheric pressure has been satisfied. Fig. 4 depicts how the pressure waves propagate along the axis of symmetry, starting from the impacted surface. These waves reach the top of the droplet at about $t^o = 0.5$ and then rebound, producing a region of negative pressure. The pressure at the stagnation point (0, 0) is positive (compressive) until the rarefaction waves reach that point along the axis of symmetry ($r = 0$) or along the impact surface ($z = 0$). Its magnitude increases continuously (until the time t^o of about 0.25) at a much greater rate than the pressures over the rest of the impacted surface. At the same time, the rarefaction wave starts to affect the pressure near the outer edge (Figs. 3 and 4). The pressure at the stagnation point then decreases, oscillates, and gradually decays. The numerical computation was terminated at $t^o = 2.5$, since the steady state has been reasonably approached, and most of the important features of the liquid-solid impact have already been disclosed. Fig. 5 also shows the pressure history at several other locations as a function of time. Since the pressure gradient on the impacted surface is the greatest near the contact edge as shown in Fig. 3, the instantaneous radial velocity increment at this location must be correspondingly the largest (Fig. 6).

Fig. 6 shows the radial velocity distribution on the impacted surface. The dotted portion of the curves indicate regions where the jetting liquid does not remain in contact with the surface. The radial jetting velocity exceeds the impact velocity at $t^o = 0.2$ for Mach 0.2 and $t^o = 0.3$ for Mach 0.5.

The positive pressure gradient in the radial direction results in a positive time-rate of change in the radial velocity. Therefore, as pressure gradients on the impacted surface change from positive to negative (Fig. 3), the radial velocities on the impacted surface change correspondingly from increasing to decreasing (Fig. 6). The maximum pressure gradient and its corresponding location on the impacted surface are given in Fig. 7. The radial pressure gradient reaches its peak at $t^o = 0.2$ just inside the initial outer edge. It then decreases to its steady-state value as the location of the maximum pressure gradient moves outward.

IV. CONCLUSIONS

The object of this research was to study the environment leading to the destructive mechanism due to a finite cylindrical jet impingement on a solid material surface. Pressure and velocity distributions were solved as a function of time for a rigid plane. The following conclusions can be drawn based on the study.

1. The impulsive motion during the very initial unsteady period generates the most destructive action.
2. Compressibility is the predominant effect on liquid solid impact.
3. The effect of assuming a non-slip, rather than free-slip boundary condition on the impacted surface , which the present authors have treated elsewhere (Ref. 5), is that the non-slip boundary condition retards the lateral flow along the solid surface. Therefore, the pressure build-up is slightly higher with the non-slip boundary condition than with the free-slip boundary condition.
4. Both the intensive high pressure at the center of impact surface and the severe radial pressure gradient on the periphery contact edge could be responsible for material damage.

ACKNOWLEDGEMENT

The work was supported by National Science Foundation Grant No. Gk. 730.

V. REFERENCES

1. Batchelor, G.K.: "An introduction to fluid dynamics". Cambridge University Press. (1967).

2. Schlichting, H.: "Boundary layer theory". McGraw-Hill. (1960).

3. Tait, P.G.: "Report on some of the physical properties of fresh water and sea water". Phys. Chem. 2, pp. 1-71. (1888).

4. Cole, R.H.: "Underwater Explosions". Dover. (1965).

5. Huang, Y.C., Hammitt, F.G., and Yang, W-J: "Normal impact of a finite cylindrical liquid jet on a flat, rigid plane". Report No. UMICH 03371-9-T, University of Michigan. (1971).

6. Huang, Y.C.: "Numerical studies of unsteady, two-dimensional liquid impact phenomena". Ph.D Thesis, University of Michigan. (1971).

7. Richtmyer, R.D. and Morton, K.W.: "Difference methods for initial value problems". Inter-Science. (1967).

8. Briggs, L.J.: "Limiting negative pressure of water". J. Appl. Phys. 21, pp. 721-722. (1967).

LIST OF FIGURES

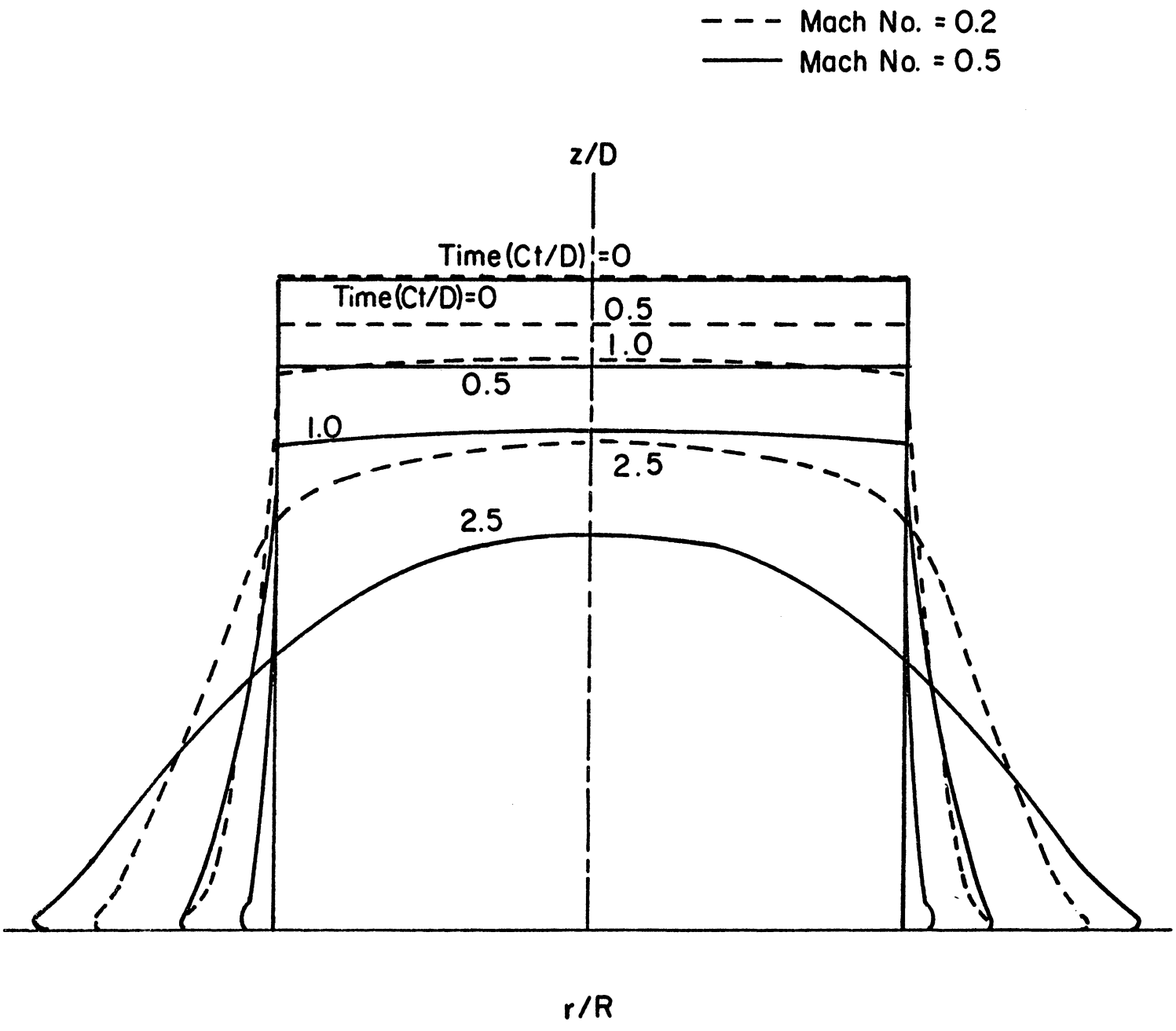

Fig. 1. Shape-Time History of an Initially Cylindrical Droplet with L/D = 1, at Mach Numbers = 0.2 and 0.5 for Non-Slip Boundary Condition.

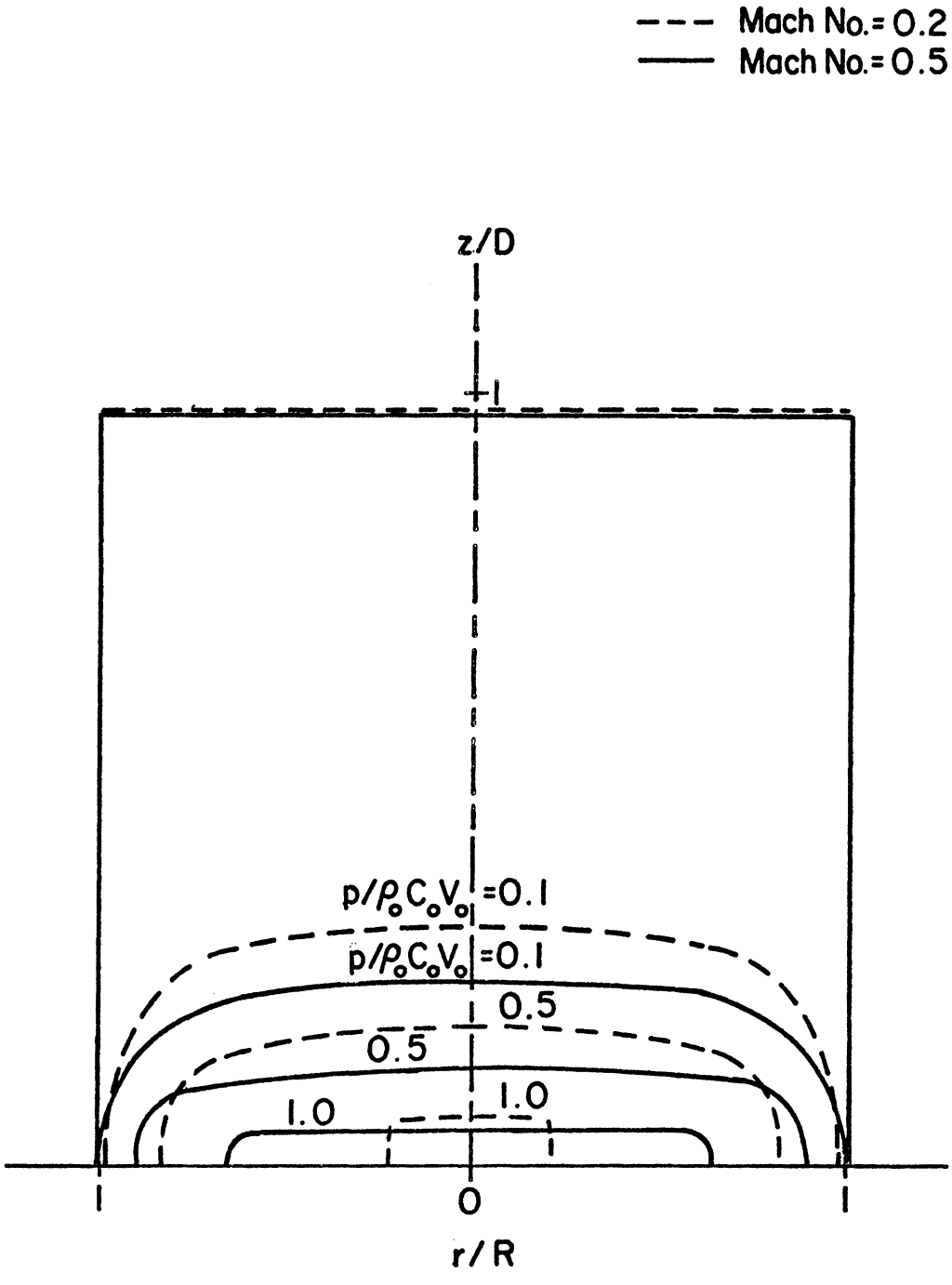

Fig. 2 a. Isobar Distribution in an Initially Cylindrical Droplet with L/D = 1, at Time (Ct/D) = 0.125, for Impact Mach Numbers of 0.2 and 0.5. Non-Slip Boundary Condition.

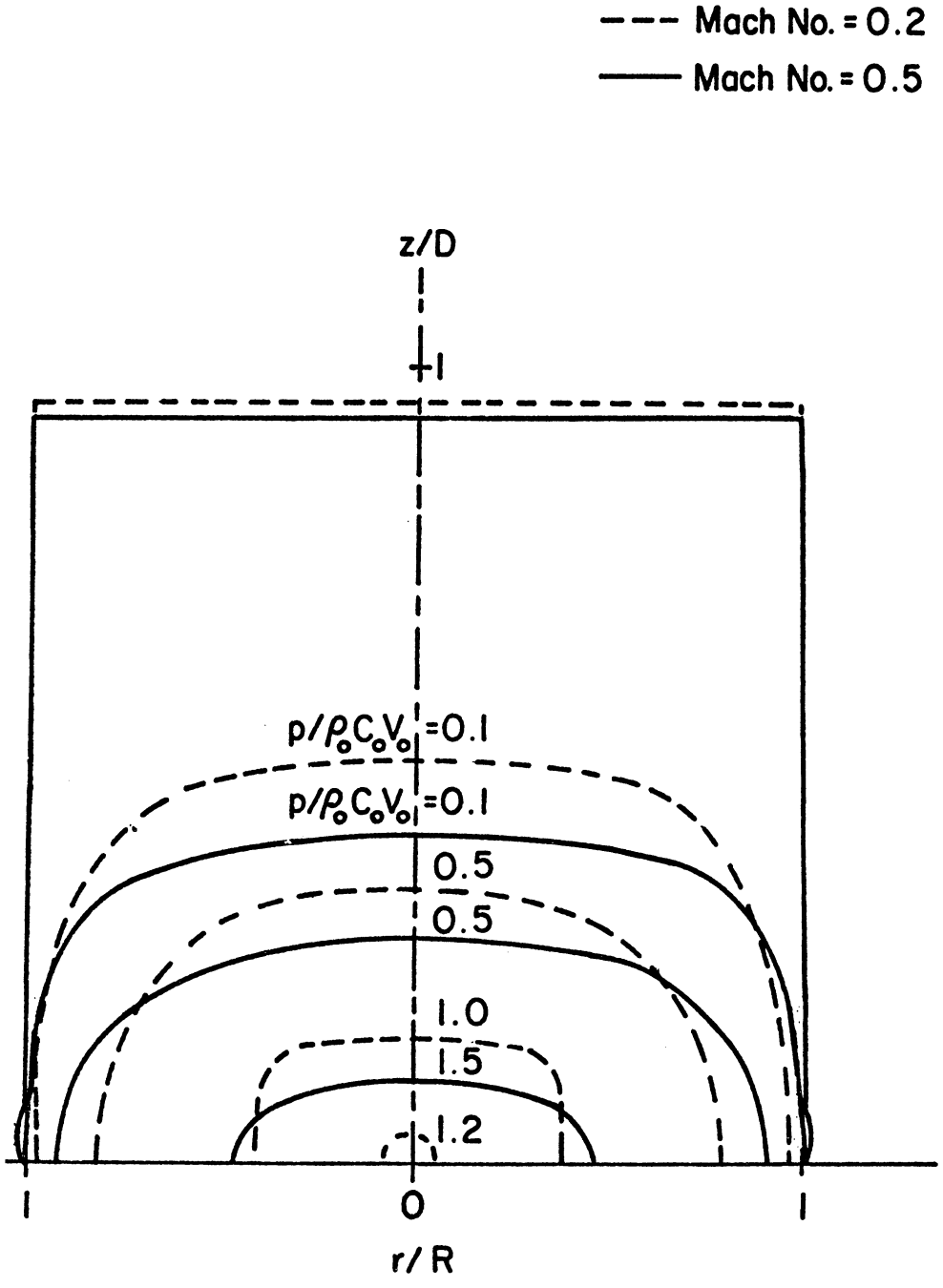

Fig. 2b. Isobar Distribution in an Initially Cylindrical Droplet with L/D = 1, at Time (Ct/D) = 0.25, for Impact Mach Numbers of 0.2 and 0.5. Non-Slip Boundary Condition.

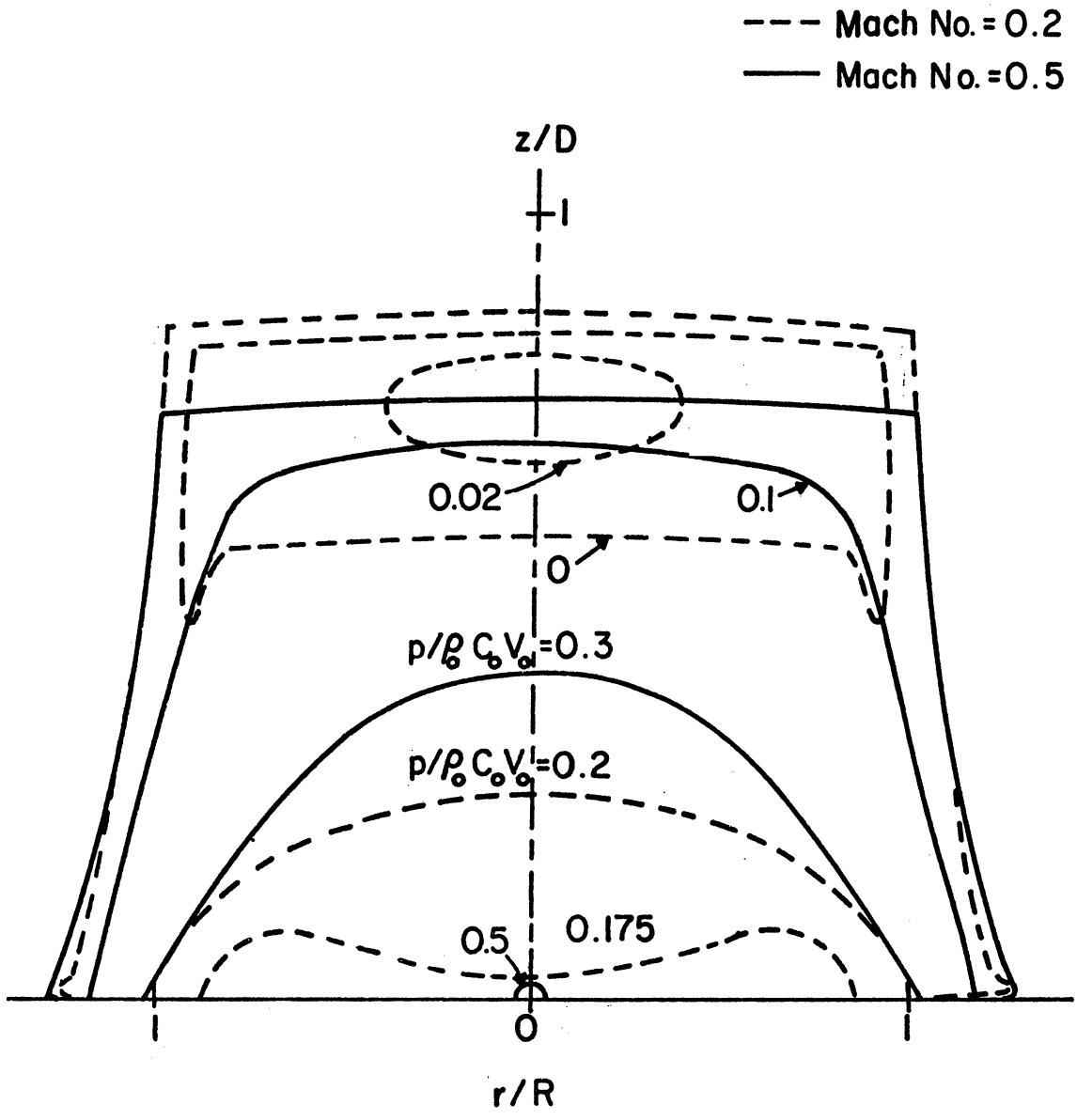

Fig. 2c. Isobar Distribution in an Initially Cylindrical Droplet with L/D = 1, at Time (Ct/D) = 1, for Impact Mach Numbers of 0.2 and 0.5. Non-Slip Boundary Condition.

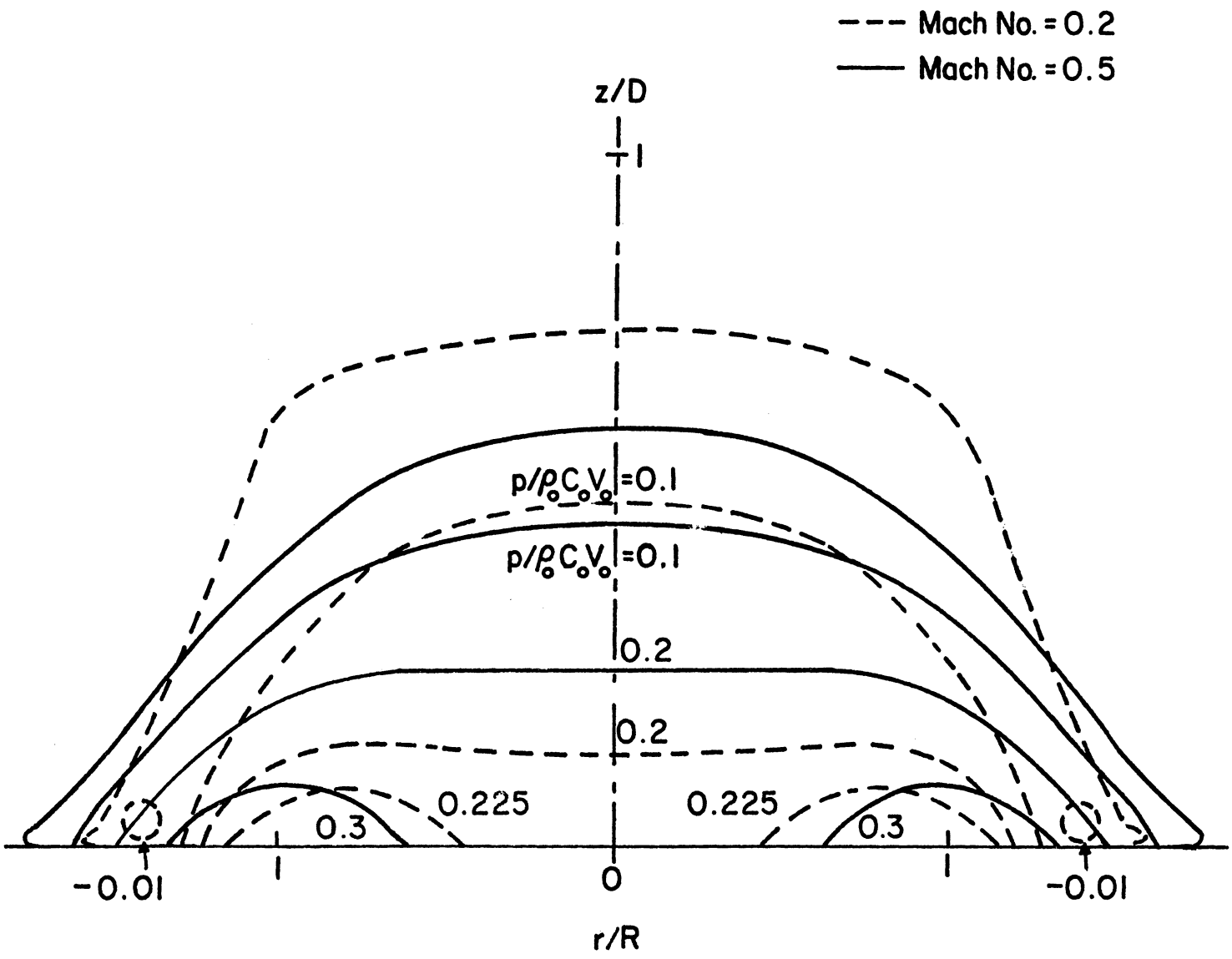

Fig. 2d. Isobar Distribution in an Initially Cylindrical Droplet with L/D = 1, at Time (Ct/D) = 2.5, for Impact Mach Numbers of 0.2 and 0.5. Non-Slip Boundary Condition.

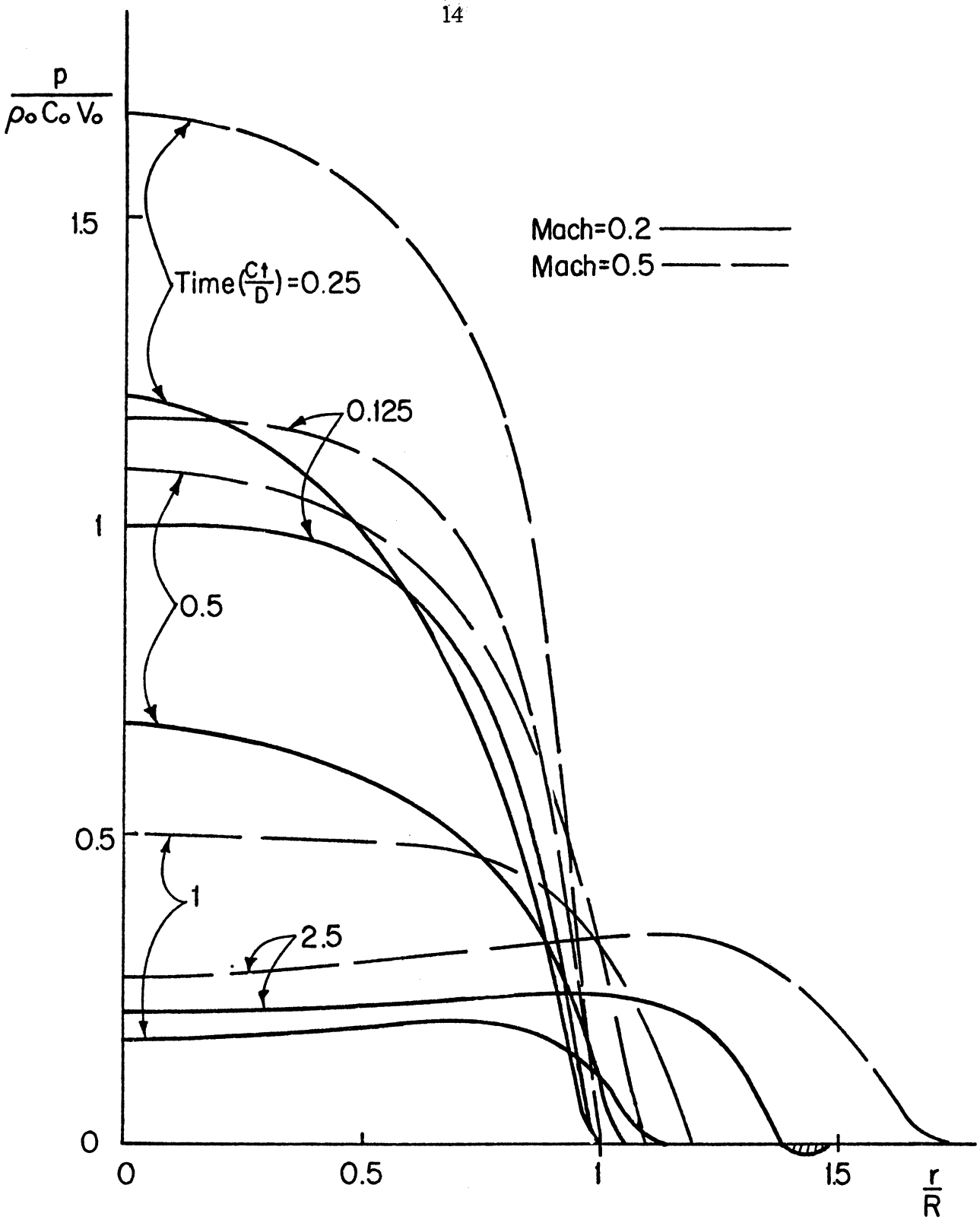

Fig. 3. Pressure-Time History at Liquid-Solid Interface (z = 0) of an Initially Cylindrical Droplet with L/D = 1, for Impact Mach Numbers of 0.2 and 0.5. Non-Slip Boundary Condition.

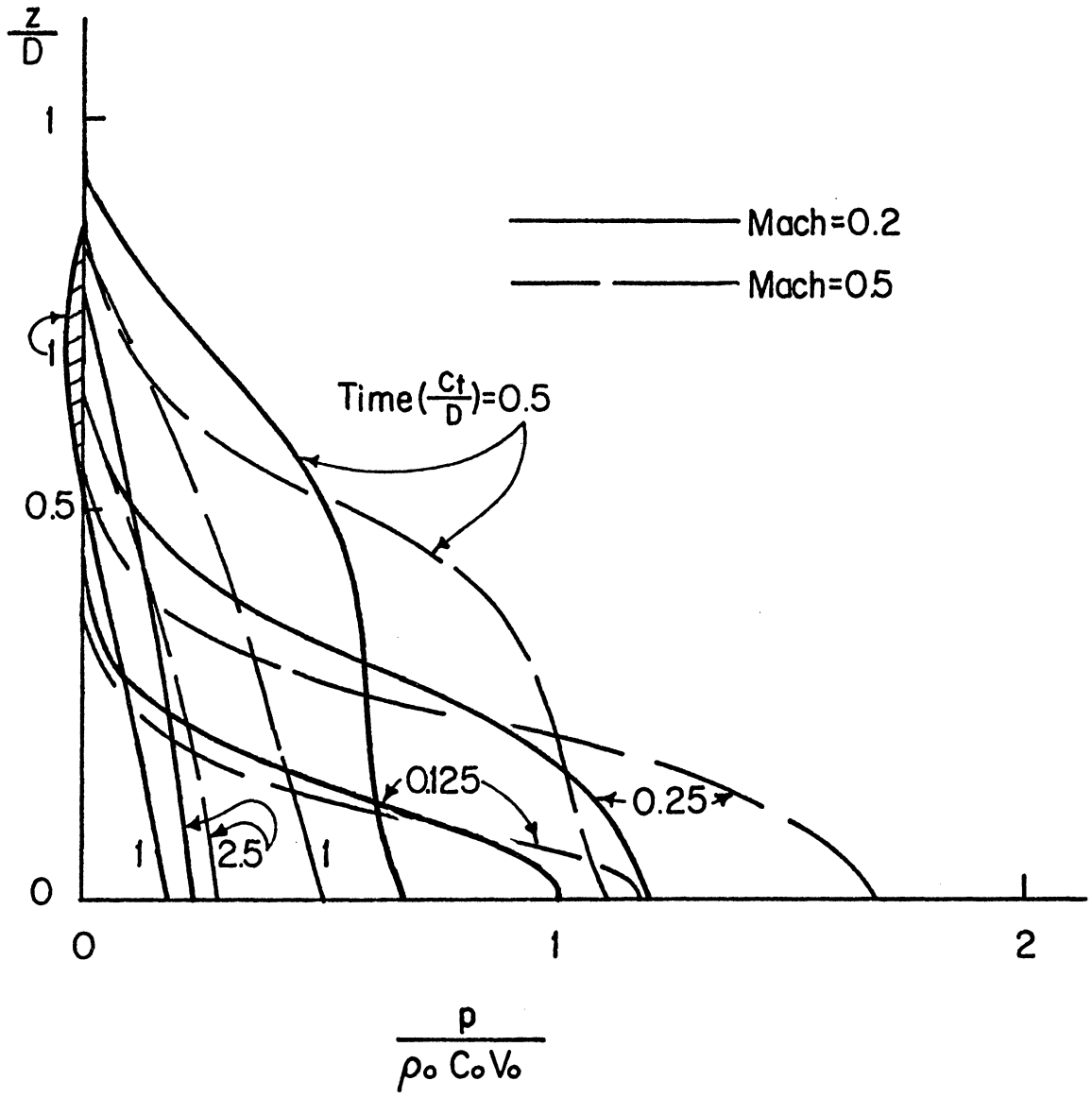

Fig. 4. Pressure-Time History along the Symmetrical Axis (r = 0) of an Initially Cylindrical Droplet with L/D = 1, for Impact Mach Numbers of 0.2 and 0.5. Non-Slip Boundary Condition.

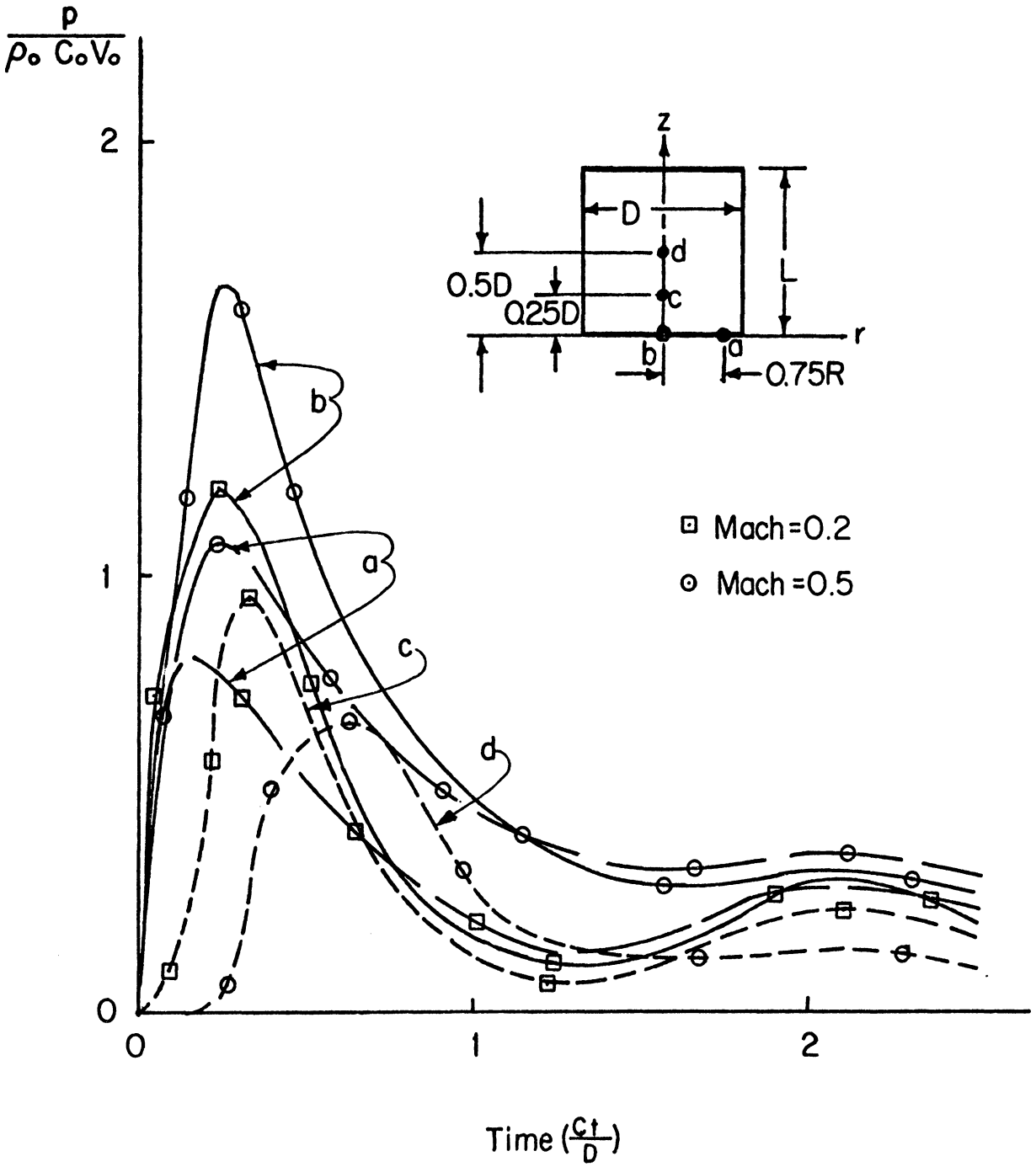

Fig. 5. Local Pressure-Time History in an Initially Cylindrical Droplet with L/D = 1 for Impact Mach Numbers of 0.2 and 0.5 and under Non-Slip Boundary Condition.

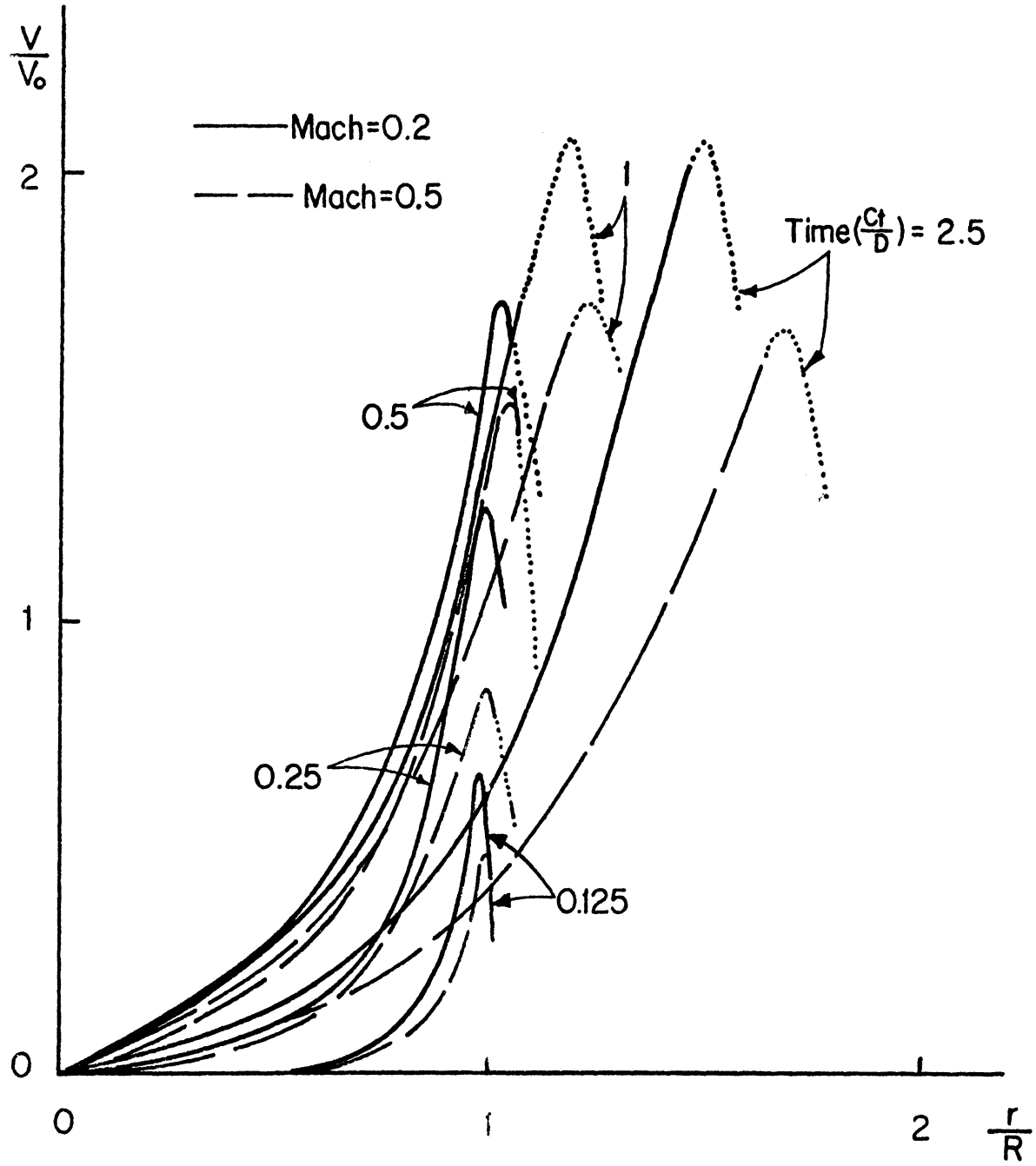

Fig. 6. Radial Velocity-Time History at Liquid-Solid Interface (r = 0) of an Initially Cylindrical Droplet with L/D = 1, for Impact Mach Numbers of 0.2 and 0.5. Non-Slip Boundary Condition.

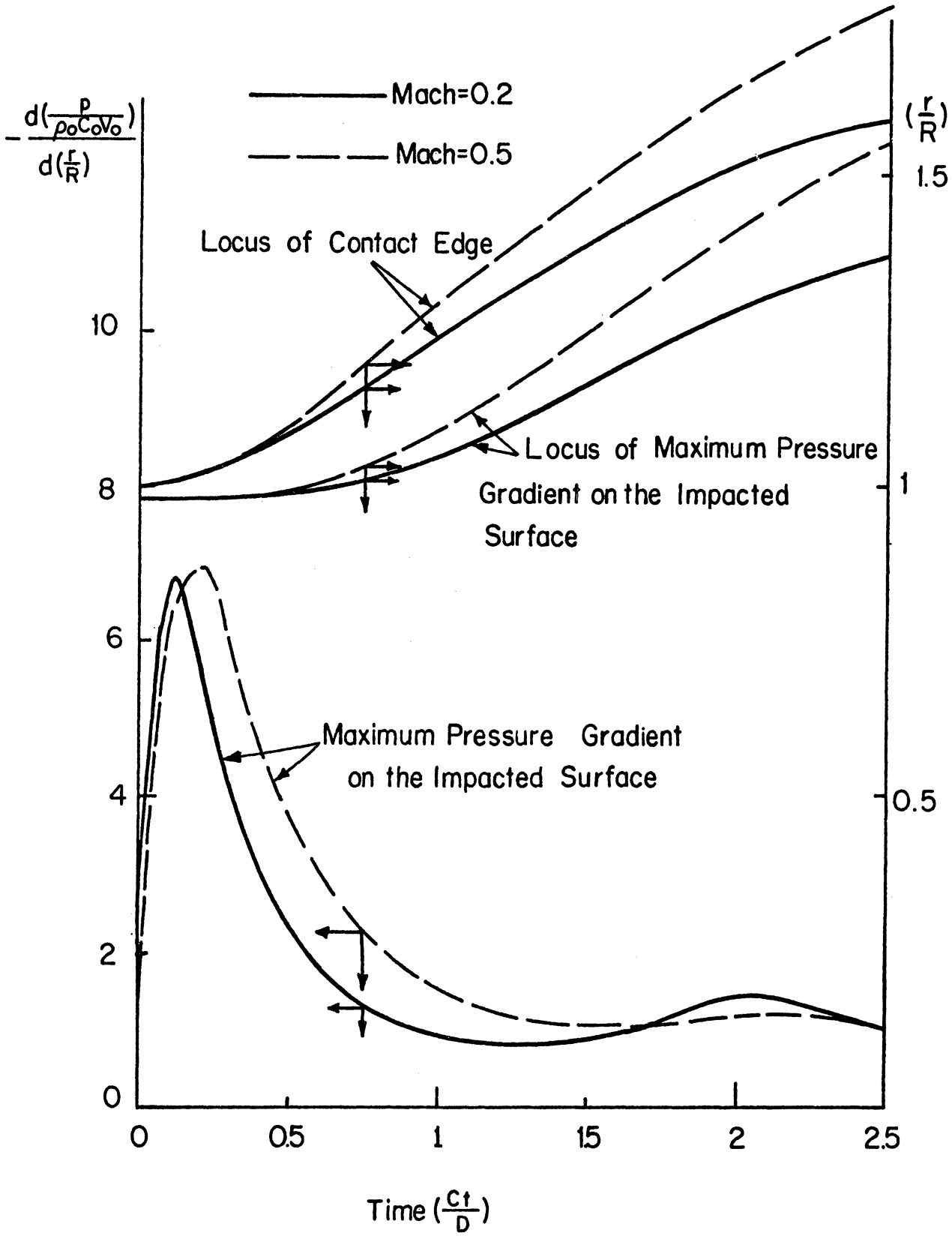

Fig. 7. Maximum Pressure Gradient-Time and -Location Relation and Contact Edge-Time History of an Initially Cylindrical Droplet with L/D = 1, for Impact Mach Numbers of 0.2 and 0.5. Non-Slip Boundary Condition.